Imaging nonlinear scatterers applying the time reversal mirror

T. J. Ulrich[a] and P. A. Johnson[b]
Los Alamos National Laboratory of the University of California, EES-11, Los Alamos, New Mexico 87545

A. Sutin[c]
Stevens Institute of Technology, Artann Laboratories

(Received 12 August 2005; revised 22 December 2005; accepted 1 January 2006)

Nonlinear elastic wave spectroscopy (NEWS) has been shown to exhibit a high degree of sensitivity to both distributed and isolated nonlinear scatterers in solids. In the case of an isolated nonlinear scatterer such as a crack, by combining the elastic energy localization of the time reversal mirror with NEWS, it is shown here that one can isolate surfacial nonlinear scatterers in solids. The experiments presented here are conducted in a doped glass block applying two different fixed frequency time-reversed signals at each focal point and scanning over a localized nonlinear scatterer (a complex crack). The results show a distinct increase in nonlinear response, via intermodulation distortion, over the damaged area. The techniques described herein provide the means to discriminate between linear and nonlinear scatterers, and thus to ultimately image and characterize damaged regions. © *2006 Acoustical Society of America.* [DOI: 10.1121/1.2168413]

PACS number(s): 43.60.Tj, 43.25.Dc, 43.40.Le, 43.40.Fz [MFH] Pages: 1514–1518

I. INTRODUCTION

Combining the time reversal mirror (TRM) with elastic nonlinearity holds great promise for isolating a nonlinear scatterer such as a crack in a solid. The TRM provides the means to narrowly focus wave energy in time and space. If the focal point is a nonlinear scatter, harmonics and other nonlinear effects are induced that are not induced elsewhere in an otherwise elastically linear solid. Thus the combination of illuminating nonlinear scatterers applying time reversal (TR) and analyzing the focused signal for nonlinear response offers the means to image them. Other wave scatterers such as sidewalls and voids do not exhibit nonlinear response.[1] In this paper we show how the method can be applied to provide a high-resolution image of a crack located on the surface of a glass block. In the following, we present pertinent background information and then describe the experiment. Following this, we present the results and discussion and then conclude.

II. BACKGROUND

Time reversal has been taken to an advanced state primarily by the group at the University of Paris VII (Laboratoire Ondes et Acoustique, ESPCI) who have comprehensively explored the underlying fundamental physics and have developed numerous applications.[2–6] TRM provides the means to focus an ultrasonic wave, regardless of the position of the initial source and regardless of the heterogeneity of the medium in which the wave propagates. TRM has a wide range of applications, including destruction of tumors and kidney stones and long-distance communication in the ocean.[7] The nondestructive evaluation (NDE) applications of (linear) TRM to date include detection of small, low-contrast defects within titanium alloys[4,5] and detection of cracks in a thin air-filled hollow cylinder.[6] In these experiments nonlinear effects were not considered.

Over the last two decades, studies of nonlinear wave methods applied to nondestructive evaluation (NDE) have demonstrated that the nonlinear elastic response of materials may radically increase in the presence of damage (cracks or other flaws).[1,8–11] Numerous applications to NDE have been developed by many groups in the US, Europe, and Russia.

TRA focusing, providing a large localized amplitude of an acoustic wave, is a good tool for investigation of nonlinear effects for the application for NDE. In the work of Montaldo *et al.*[12] the second harmonic generation in the TRA focused signal in homogeneous fluid media was observed. Here we employ nonlinear interaction of the TRA focused signal with a crack in a solid (i.e., a highly nonlinear scatterer) for crack detection purposes applying the wave modulation technique. To our knowledge the experiment described here and its predecessors[13,14] are the first to implement nonlinear time reversal and apply it to NDE and imaging in solids.

III. EXPERIMENTAL DETAILS

One of the most straightforward methods to evaluate the nonlinear elastic response of a material is to measure the modulation of an ultrasonic wave (f_{hi}) by a low-frequency vibration (f_{lo}). This gives rise to nonlinear wave mixing in materials with distributed (e.g., a rock) or localized damage (e.g., a crack in a solid) where the spectral composition contains both pure tones (f_{lo} and f_{hi}) as well as sum and difference frequencies ($f_+ = f_{lo} + f_{hi}$ and $f_- = f_{hi} - f_{lo}$), while an undamaged (elastically linear) material would simply exhibit the pure tones. These additional frequencies in the signal (f_+

[a]Electronic address: tju@lan1.gov
[b]Electronic address: paj@lan1.gov
[c]Electronic address: asutin@stevens-tech.edu

 0001-4966/2006/119(3)/1514/5/$22.50

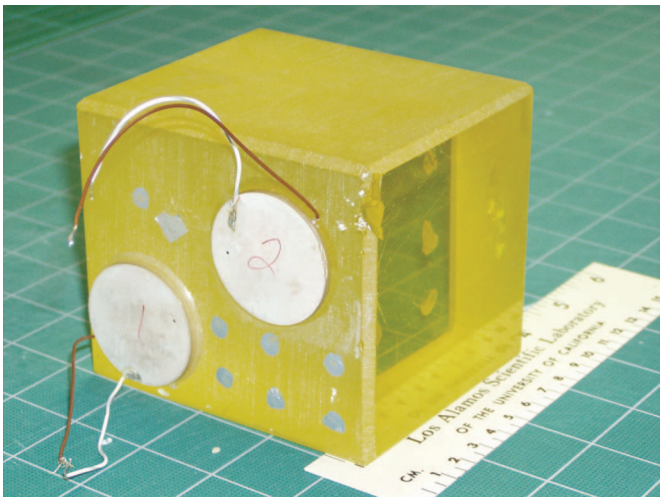

FIG. 1. Doped glass block showing the attached sources. The sources are located approximately symmetrically about the crack on the opposing face. A cm scale is located on the right of the sample.

and f_-) are usually referred to as sidebands of the high frequency because $f_{lo} \ll f_{hi}$, and thus the sum and difference frequencies lie equally and closely spaced about f_{hi}. In principle, however, the only requirement is that f_{lo} and f_{hi} are different enough to resolve, thus f_+ and f_- do not necessarily lie close to f_{hi} as is typical of the concept of sidebands. This is true of the frequencies used in the experiment presented here ($f_{lo}=170$ kHz, $f_{hi}=255$ kHz, $f_+=425$ kHz, and $f_-=85$ kHz). These frequencies were chosen from the sample's natural frequencies by selecting the frequencies corresponding to the highest amplitudes in response to a broadband pulse.

The experiment was conducted in a doped glass block of dimensions $101\times89\times89$ mm ($\rho\approx3.0$ g/cm^3, $c\approx2.5$ km/s, $Q\approx2000$). Two piezoelectric ceramics (PZT-5a, 38 mm diameter, 2.8 mm thickness) were used as sources. The sources were bonded to the face of the glass block opposite to the crack location. Photographs of the sample are found in Figs. 1 and 2, showing the cracked face and attached ceramics. The elastic response on the cracked face was measured using a broadband (DC to 1.5 MHz) laser vibrometer (Polytec model OFV 303, controller OFV 3001, velocity range 1 V=1 m/s). A block diagram of the apparatus is shown in Fig. 3.

Each source was driven with a different frequency [$f_1=f_{lo}=170$ kHz and $f_2=f_{hi}=255$ kHz, signal lengths $\tau=0.1$ ms, sinusoidal envelope, see Fig. 4(a)]. The direct signal was measured for each source independently and then time reversed. This experiment differs from standard TR experiments as the direct time-reversed signals were then input back at the original source locations, as was done in other work.[15–17] Reciprocity dictates that the resulting signal will focus at the point of the original detector.[18] This fact allows for the use of multiple low-amplitude channels to produce a focused (in space and time) high-amplitude response at any point in the solid. In these experiments we restrict ourselves to focusing on the surface of the sample; as such, the crack analyzed here is a surface crack with a penetration depth of a few millimeters.

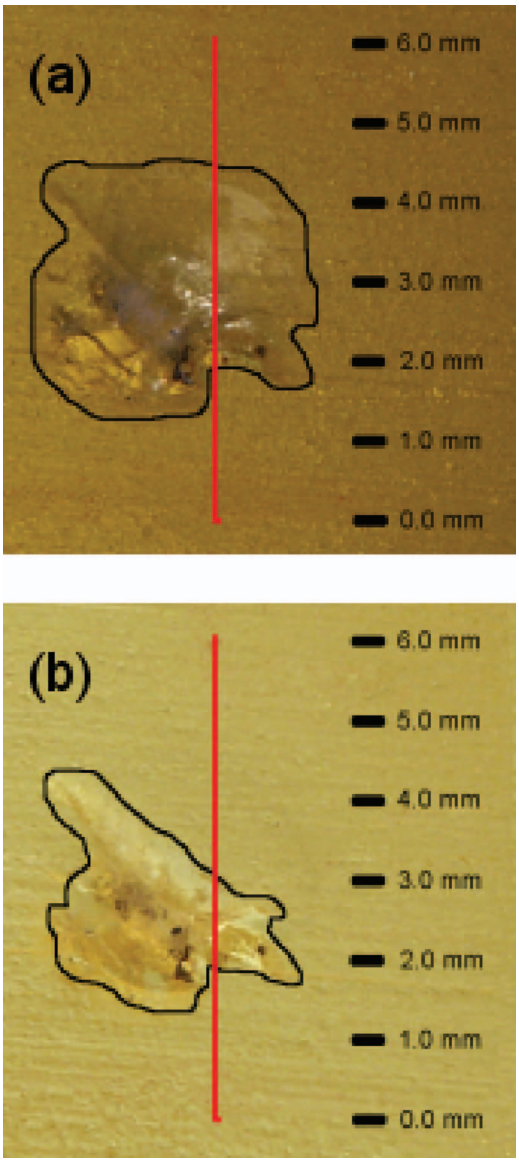

FIG. 2. Close-up of the crack in the doped glass block (a) lit from the surface and (b) backlit through the glass. The vertical red line indicates the path along which the measurements were made. The visually apparent extent of the crack is denoted by the black outline encircling the cracked region. The two lighting techniques illuminate different features: the surface lighting illuminates the two-dimensional surfacial features while the backlighting highlights the third dimension of depth but eliminates some of the surface detail. Notice the difference in apparent crack extent with the change of lighting as well as the obvious complexity of the crack (e.g., crack shape and density variations).

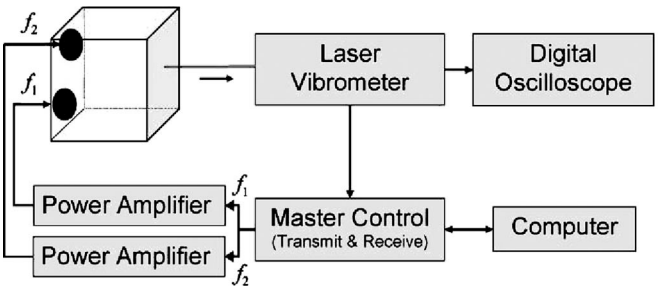

FIG. 3. Block diagram of the nonlinear TRA (NTRA) experimental system.

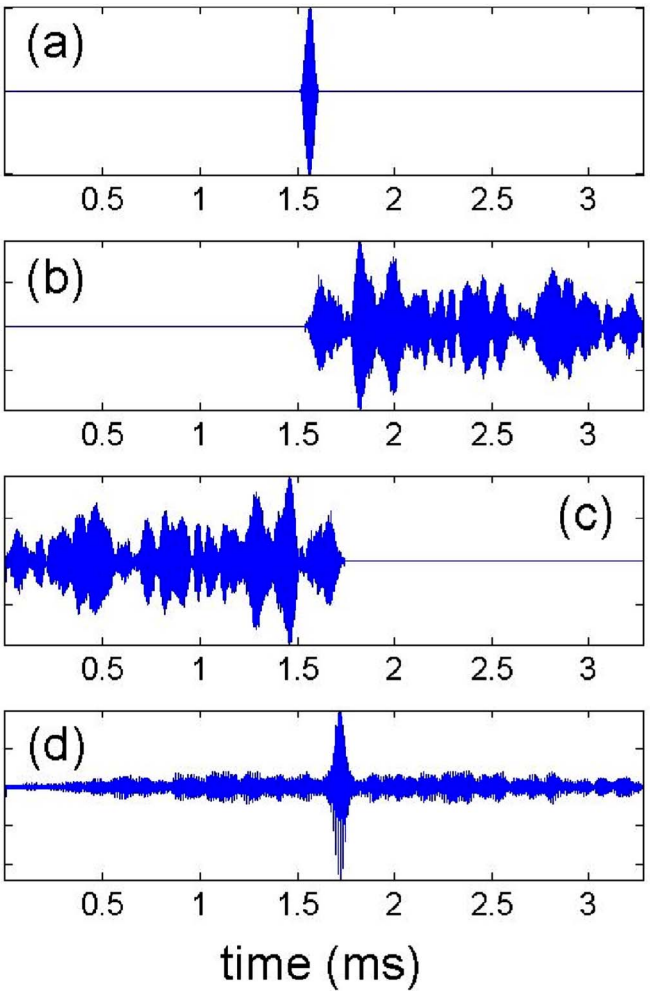

FIG. 4. (Color online) Waveforms from the TR experiment: (a) Input signal $s_n(t)$ for f_1 ($n=1$, f_2 not shown); (b) signal received at the point of detection $r_{m,n}(t)$ (from the f_1 source); (c) TR signal $r_{m,n}(-t)$ input to the transducer at the location of the original source f_1; and (d) focused signal R_m at the original point of detection due to the transmission of the TR signals [i.e., (c) and the analogous signal from f_2, not shown].

The experimental protocol of the nonlinear TR method used in this experiment is as follows:

(1) Transmit signal $s_n(t)$ from source n, Fig. 4(a),

$$s_n(t) = U_n \cos(2\pi f_n t) \sin^2\left(\frac{\pi t}{\tau}\right), \tag{1}$$

where f_n is the frequency transmitted from the nth transducer with a maximum amplitude U_n and duration τ.

(2) Receive the signal $r_{m,n}(t)$ at the selected point x_m (i.e., focal point of the laser vibrometer) on the sample for each f_n independently, e.g., Fig. 4(b).

(3) Time reverse the received signals, Fig. 4(c),

$$r_{m,n}(t) \rightarrow r_{m,n}(-t). \tag{2}$$

(4) Simultaneously transmit the amplified TR signals $S_{m,n}(t)$ from their original source locations,

$$S_{m,n}(t) = U_n \frac{r_{m,n}(-t)}{\max(r_{m,n}(-t))}, \tag{3}$$

where the U_n's are the same maximum amplitudes used in step 1.

(5) Record the TR focused signal $R_m(t)$ at the mth focal point of the laser vibrometer (x_m), Fig. 4(d),

$$R_m(t) = \sum_{n=1}^{N} \int_0^{t_{\text{final}}} dt' G(x_m t | x_n t') S_{m,n}(t'). \tag{4}$$

N is the total number of source transducers, x_n is the location of the nth transducer, and $G(x_m t | x_n t')$ is the Green's function taking the signal transmitted from location x_n and time t' to point x_m at a later time t. The integration is taken over the entire length of the waveform from 0 ms to t_{final} = 3.2768 ms (i.e., 32 768 samples taken at 10 MS/s).

(6) Move the laser focal point to the next desired location (x_{m+1}) and repeat the process for M total focal points.

The above steps are the generalized procedure followed for the scan presented in this paper. In this experiment a scan (in one dimension) was conducted across the cracked area. At each of the $M=22$ points (x_m) the same two (i.e., $N=2$) f_1 and f_2 sources were used. Additionally the drive amplitudes and durations remained constant at $U_1=40$ V, $U_2=100$ V, and $\tau=100$ μs, as did the source locations x_1 and x_2, as the transducers were bonded to the surface of the sample. The difference in the drive amplitudes U_1 and U_2 arises due to the use of two different amplifiers with differing gain. The focal point resolution (i.e., spot size of the laser) is ~ 10 μm. Scanning across the crack was done with graduated increments. In and near the cracked region the step size was consistently 200 μm, while away from the crack the step size varied from 200 to 500 μm. The path of the one-dimensional scan can be seen in Fig. 2.

IV. RESULTS AND DISCUSSION

The waveforms of the focused signals were saved at each focal point and analyzed for the presence of nonlinear scattering as well as other characteristic features that may be present. This was done by first comparing the complete set of unfiltered waveforms as a function of position [Fig. 5(a)]. Subsequently, these waveforms were then filtered about the frequencies corresponding to the sum and difference frequencies and again compared as a function of position [Figs. 5(b) and 5(c)]. The cracked region was visually measured to be in the range of $\sim$1.9–4.4 mm along the scan path (Fig. 2). The amplitudes of the focused waveform are found to increase near the region of the crack as do the sidelobe amplitudes. By comparison, the nonlinear features exhibit narrower focusing, indicating the extent of the crack boundaries (Fig. 5). In addition, the sum and difference frequencies display different behavior inside the crack. As the signal is focused at different locations along the crack, the difference frequency waveforms become more structured in amplitude than the sum frequency waveforms and exhibit more sidelobes [Fig. 5(b), positions 1.9–4.4 mm]. While this is still under investigation, it may relay information about the internal structure of the crack.

A spectral analysis of the waveforms was performed at each position to investigate the possibility of other frequencies being present in the signal (Fig. 6). The two primary frequencies are clearly observed through the entire scan and the sum and difference frequencies are seen inside the crack.

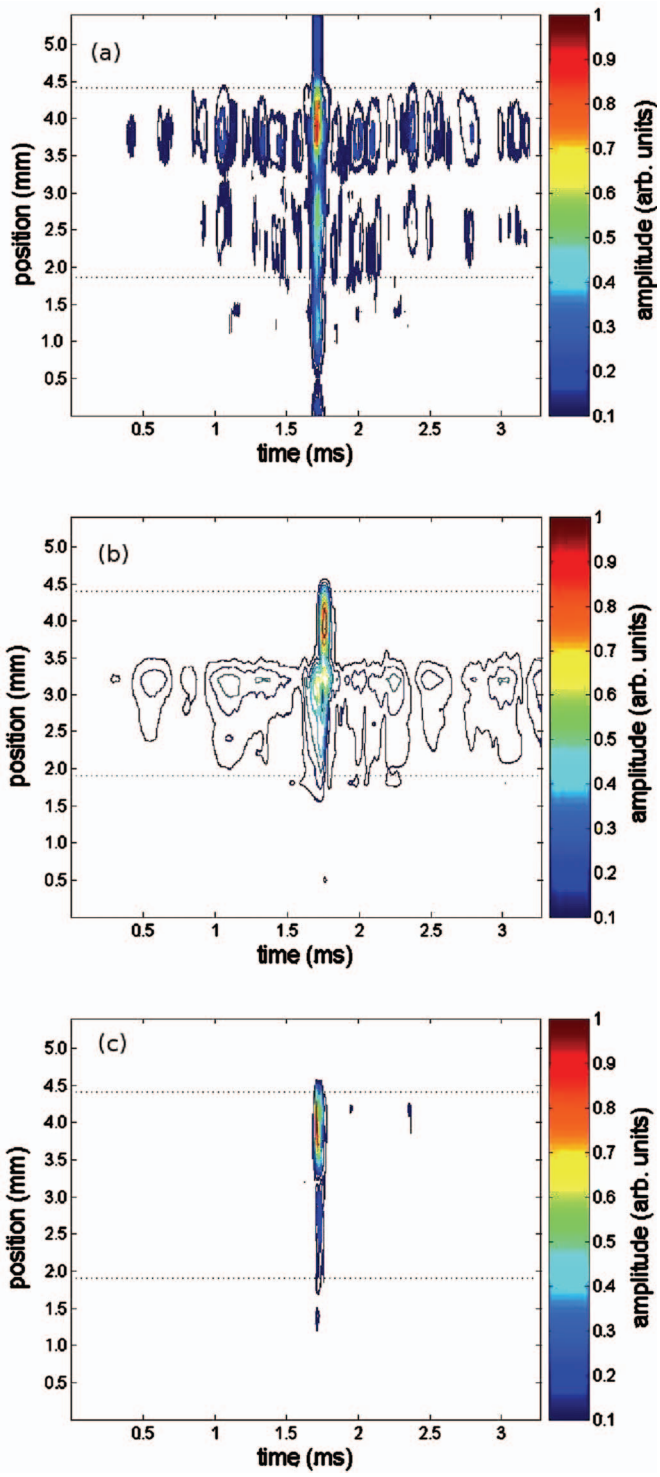

FIG. 5. Focused signal waveforms R_m at each focal position. The amplitudes of the waveforms increase in the damaged region (denoted by horizontal dotted lines), as well as gain more structure in the focused signal (i.e., the residual temporal lobes). (a) Unfiltered waveform; (b) waveform filtered about the difference frequency (f_-=85 kHz) with a bandwidth of 8.5 kHz (i.e., 10% of the filtered frequency); and (c) waveform filtered about the sum frequency f_+=425 kHz with a bandwidth of 42.5 kHz (i.e., 10% of the filtered frequency).

This plot also shows energy at 510 kHz, which is both $3f_1$ and $2f_2$. The image also shows complexity in broadening of energy around especially f_2 at two locations along the scan inside the cracked region for reasons that may have to do with crack complexity.

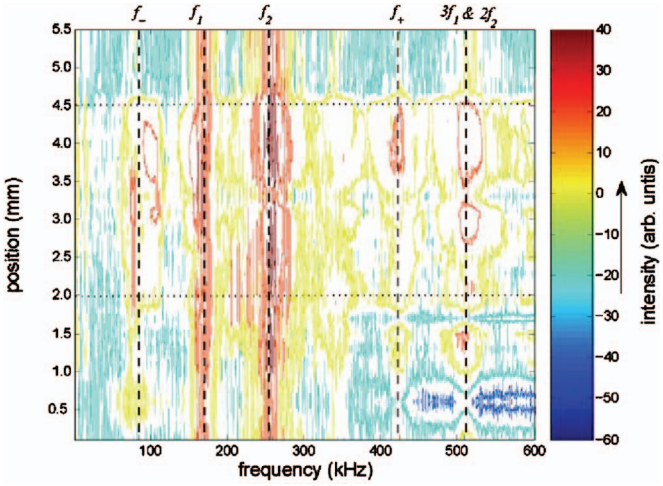

FIG. 6. Frequency components in the focused signal at each focal position. Notice the addition of sum ($f_+=f_1+f_2$=425 kHz) and difference ($f_-=f_2-f_1$=85 kHz) frequencies and harmonics (e.g., 510 kHz) in the damaged region. Frequencies of note are indicated by a vertical dashed line. The approximate extent of the damaged region is depicted by the horizontal dotted lines.

Three prominent features are of note in the focused waveforms. (1) The amplitudes of the waveforms in and around the crack are markedly higher than at points away from the crack (Fig. 5). (2) Waveforms in the cracked region contain the nonlinear signature of sum and difference frequency spectral components [Figs. 5(b), 5(c), and 6]. (3) In portions of the crack the TR focused signal is highly structured in its amplitude, i.e., large sidelobe amplitudes relative to the primary focused signal amplitude [Figs. 5(a), 5(b), and 7].

The additional structure of the residual temporal lobes (or sidelobes) in the TR focused waveforms is not simply a signal-to-noise issue where the sidelobes become more visible due to the increased amplitudes of the signals in the damaged area, rather, the amount of energy in these lobes E_{lobes} (in comparison to the total energy E_{total}) is much greater in the damaged/nonlinear region ($E_{\text{lobes}}/E_{\text{total}} \approx 0.88$) than in the undamaged material as ($E_{\text{lobes}}/E_{\text{total}} \approx 0.36$). The energy ratios at each point m were calculated as

$$\left.\frac{E_{\text{lobes}}}{E_{\text{total}}}\right|_m = 1 - \frac{\Sigma_{j=\alpha}^{\beta} R_m^2(t_j)}{\Sigma_{i=1}^{N_S} R_m^2(t_i)}, \tag{5}$$

where N_S is the number of samples in the waveform; α and β are the indices corresponding to the width of the initial pulse centered around the time of focus (t_{focus}=1.55 ms) thus defining the red portions of Fig. 7. All other parameters are as previously defined. The reason for the bleeding of the total energy into the sidelobes is unknown. One speculation is that this is further confirmation of nonlinearity of the signal through a nonlinear attenuation mechanism, such as that seen in rocks.[19] One nonlinear effect connected with interaction of the high-amplitude TRA focused wave with a crack is amplitude-dependent attenuation. This nonlinear attenuation leads to the decrease of the relative levels of the primary focused signal (Fig. 7, red portion) to the sidelobe amplitudes (Fig. 7, blue por-

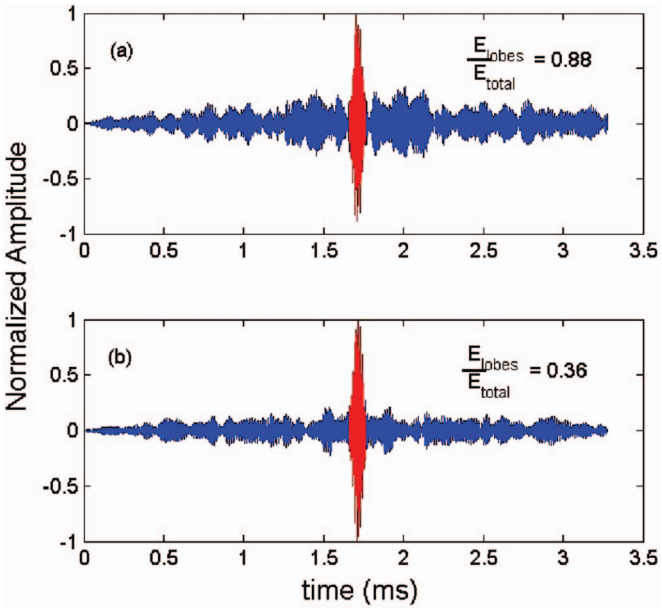

FIG. 7. TR focused waveforms (a) inside the crack and (b) outside the crack. The temporal sidelobes (blue) of the focused signal contain more energy in the cracked region (a) than outside of the crack (b). The width of the original signal [i.e., $s_n(t)$] is shown in red. In a perfect TR focusing the original source(s) would be reconstructed in time and space, thus the red portion of the plots (the primary focusing) is chosen to be the width of the original signal. The ratio of the energy in the temporal lobes (E_{lobes}) to the total energy of the signal (E_{total}) is given for each signal in the corresponding frame.

tion) of the TRA signal in the cracked area. This amplitude could be less than relative amplitude of the TRA signal out of the crack where there is no nonlinear attenuation.

While the presence of nonlinear components of the waveform in the damaged area did not come as a surprise, we were, however, surprised at the degree of amplification of the entire focused signal on the nonlinear scatter. We presume this is due to amplification due to the cracked region having the ability to oscillate freely, independent of bulk response. It appears that this effect is the result of the cracked surface having a tenuous connection to the block, thus focusing the same amount of acoustic energy upon the crack as was focused at an undamaged location, which will result in a greater amplitude, as we see here. The general amplification of the overall signature may then be a surface effect and one not expected in a nonlinear scatterer located internally; however, the presence of wave mixing and harmonics should be present.

We are continuing investigations into the effects of sample geometry, transducer locations, source amplitude effects, as well as the further study of the crack features presented in this paper. The development of a two-dimensional automated scanning system for full surface imaging is also underway to image surface cracks with a resolution of $\sim 10\ \mu$m. Additional efforts are being directed into probing subsurface damage features as well as intrinsic nonlinear properties in three-dimensional elastic solids.

ACKNOWLEDGMENTS

We are grateful to James TenCate and Robert Guyer. This research was supported in part by institutional support (LDRD) at the Los Alamos National Laboratory and by the United States Air Force Office of Scientific Research.

[1]P. A. Johnson, "The new wave in acoustic testing," Mater. World **7**, 544–546 (1999).
[2]M. Fink, D. Cassereau, A. Derode, C. Prada, P. Roux, M. Tanter, J. L. Thomas, and F. Wu, "Time-reversed acoustics," Rep. Prog. Phys. **63**, 1933–1995 (2000).
[3]M. Fink, "Time reversed acoustics," Sci. Am. **281**, 91–113 (1999).
[4]C. Prada, E. Kerbat, D. Cassereau, and M. Fink, "Time reversal techniques in ultrasonic nondestructive testing of scattering media," Inverse Probl. **18**, 1761–1773 (2002).
[5]N. Chakroun, M. Fink, and F. Wu, "Time reversal processing in nondestructive testing," IEEE Trans. Ultrason. Ferroelectr. Freq. Control **42**, 1087–1098 (1995).
[6]E. Kerbrat, D. Clorennec, C. Prada, D. Royer, D. Cassereau, and M. Fink, "Detection of cracks in a thin air-filled hollow cylinder by application of the d.o.r.t. method to elastic components of the echo," Ultrasoni. Int. **40**, 715–720 (2002).
[7]W. A. Kuperman, W. S. Hodgkiss, H. C. Song, T. Akal, C. Ferla, and D. R. Jackson, "Phase conjugation in the ocean: Experimental demonstration of an acoustic time-reversal mirror," J. Acoust. Soc. Am. **103**, 25–40 (1998).
[8]O. Buck, W. Morris, and J. Richardson, "Acoustic harmonic generation at unbonded interfaces and fatigue cracks," Appl. Phys. Lett. **33**(5), 371–373 (1978).
[9]J. Cantrell and W. Yost, "Acoustic harmonic-generation from fatigue-induced dislocation dipoles," Philos. Mag. A **69**(2), 315–326 (1994).
[10]K. Van Den Abeele, P. Johnson, and A. M. Sutin, "Non-linear elastic wave spectroscopy (news) techniques to discern material damage. Part i: Nonlinear wave modulation spectroscopy," Res. Nondestruct. Eval. **12**(1), 17–30 (2000).
[11]K. Van Den Abeele, J. Carmeliet, A. Sutin, and P. Johnson, "Micro-damage diagnostics using nonlinear elastic wave spectroscopy (news)," NDT & E Int. **34**, 239–248 (2001).
[12]G. Montaldo, D. Palacio, M. Tanter, and M. Fink, "Time reversal kaleidoscope: A smart transducer for three-dimensional ultrasonic imaging," Appl. Phys. Lett. **84**, 3879–3881 (2004).
[13]A. M. Sutin, P. A. Johnson, and J. A. TenCate, "Development of nonlinear time reverse acoustics (nltra) for applications to crack detection in solids," in *Proceedings of the 5th World Congress on Ultrasonics* (2003), pp. 121–124.
[14]A. M. Sutin and P. A. Johnson, "Nonlinear elastic wave nde ii. nonlinear wave modulation spectroscopy and nonlinear time reversed acoustics," Rev. Prog. Quant. Nondestr. Eval., edited by Thompson, D. and Chimenti D., **248**, 377–384 (2005).
[15]C. Draeger and M. Fink, "One-channel time reversal of elastic waves in a chaotic 2d-silicon cavity," Phys. Rev. Lett. **79**, 407–410 (1997).
[16]C. Draeger, J.-C. Aime, and M. Fink, "One-channel time-reversal in chaotic cavities: Experimental results," J. Acoust. Soc. Am. **105**, 618–625 (1999).
[17]A. M. Sutin, J. A. TenCate, and P. A. Johnson, "Single-channel time reversal in elastic solids," J. Acoust. Soc. Am. **116**, 2779–2784 (2004).
[18]T. J. Ulrich and R. A. Guyer, "Dispacement field reciprocity in linear and nonlinear reverberant cavities: an experimental exploration with implications for time reversed acoustics," in review (2006).
[19]P. A. Johnson and A. M. Sutin, "Slow dynamics and anomalous nonlinear fast dynamics in diverse solids," J. Acoust. Soc. Am. **117**, 124–130 (2005).